A luminescence study of $Cu_2ZnSnSe_4$/Mo/glass films and solar cells with near stoichiometric copper content

M.V. Yakushev[1,2,3], M.A. Sulimov[1,3], J. Márquez-Prieto[4], I. Forbes[4], P.R. Edwards[1], V.D. Zhivulko[5], O.M. Borodavchenko[5], A.V. Mudryi[5], J. Krustok[6] and R.W. Martin[2]

[1]M.N. Miheev Institute of Metal Physics of UB RAS, 18 S. Kovalevskaya Street, 620108, Ekaterinburg, Russia
[2]Department of Physics, SUPA, University of Strathclyde, Rottenrow 107, G4 0NG Glasgow, United Kingdom
[3]Ural Federal University, Mira 19, 620002 Ekaterinburg, Russia
[4]Northumbria Photovoltaic Application Group, Faculty of Engineering and Environment, Northumbria University, Ellison Place, Newcastle upon Tyne NE1 8ST, United Kingdom
[5]Scientific-Practical Material Research Centre of the National Academy of Science of Belarus, P.Brovki 19, 220072 Minsk, Belarus
[6]Tallinn University of Technology, Ehitajate tee 5, 19086 Tallinn, Estonia

E-mail: michael.yakushev@strath.ac.uk

Abstract

$Cu_2ZnSnSe_4$ (CZTSe) is one of the leading candidates for the absorber layer in sustainable solar cells. Thin films of CZTSe with a near stoichiometric [Cu]/[Zn+Sn] were used to produce solar cells with conversion efficiency η = 6.4% by a standard solar cell processing including KCN etching and the deposition of CdS and ZnO. Both CZTSe films and solar cells were examined using photoluminescence (PL) to analyse the nature of radiative recombination and photoluminescence excitation (PLE) at 4.2 K to determine the bandgap (E_g). Low temperature PL spectra of the films reveal an intense band P1 at 0.81 eV and a low intensity band P2 at 0.93 eV. Their temperature and excitation intensity dependencies suggest that they both involve recombinations of free electrons with holes localised at acceptors with the energy level influenced by potential fluctuations in the valence band. We associate P1 and P2 with different fractions of CZTSe: with a lower and higher degree of order of Cu and Zn on the cation sub-lattice, respectively. Device processing reduced the intensity of P1 by 2.5 whereas the intensity of P2 increased by a 1.5. We assign this to a low temperature annealing due to CdS and ZnO deposition which increased the fraction of CZTSe with high degree of Cu/Zn order and decreased the fraction with low degree of Cu/Zn order. Device processing increased E_g, blue shifted P1, decreased its width, *j*-shift and the mean depth of potential fluctuations. These can also be related to the annealing and/or KCN etching and the chemical effect of Cd, due to CdS replacing copper at the CdS-CZTSe interface layer. Processing induced a new broad band P3 at 1.3 eV (quenching with E_a = 200 meV) which we attributed to defects in the CdS layer.

1. Introduction

The semiconductor $Cu_2ZnSnSe_4$ (CZTSe) is a promising replacement for $Cu(In,Ga)Se_2$ (CIGSe) in the absorber layer of thin film solar cells [1]. After achieving a record conversion efficiency of 11.6% [2] CZTSe has been considered to be one of the leading candidates for sustainable photovoltaics (PV) due to the abundance of its constituent elements in the earth's crust, their relatively low costs, toxicity and an opportunity to tune the bandgap by alloying CZTSe with Cu_2ZnSnS_4 (CZTS) [3].

The substitution of In and Ga in the chalcopyrite lattice of CIGSe with alternating Zn and Sn changes the structure to kesterite [4]. Although the electronic properties of CZTSe retain a degree of similarity to those of CIGSe the substitution makes the chemistry of defects in CZTSe significantly more complicated than that in CIGSe [5,6]. Intrinsic defects are blamed for the small value of the open circuit voltage (V_{OC}) in CZTSe-based solar cells [7,8]. Therefore, the clarification of the nature of such defects in CZTSe thin films is an important condition for further progress in the development of CZTSe-based solar cell technologies.

As with CIGSe *p*-type doping of CZTSe absorbers is attributed to intrinsic defects generated by significant deviations from the ideal stoichiometry. In CIGSe the [Cu]/[In+Ga] ratio is shifted towards copper deficiency to facilitate the formation of copper vacancies V_{Cu} which are believed to be the main doping acceptors in this material [9]. The deep donors, generated in CIGSe with excess of In/Ga, namely indium on copper sites In_{Cu}, are electrically passivated by the formation of the defect complex $2V_{Cu}+In_{Cu}$. This compensates these donors and makes it possible to employ CIGSe for the fabrication of electronic devices. Similar mechanisms for the formation of neutral defect complexes have been proposed in CZTSe using density functional theory (DFT) [6].

Correlations of the reported elemental composition of CZTSe absorber layers with the solar cell performance [6,10] suggest that conversion efficiencies in excess of 5% can be achieved at significant copper deficiency and zinc excess compositions. At such compositions the probability of formation of V_{Cu},

which according to DFT calculations [6] is the shallowest acceptor, is high and thus this defect is a likely candidate for the role of acceptor in the most efficient solar cells [2,8,11]. Also, the shallow donor, formed by zinc at copper position Zn_{Cu}, has a high probability of formation (at compositions with zinc excess) and is likely to combine with V_{Cu} to form $V_{Cu}+Zn_{Cu}$ defect complexes or A-defects [10,12]. These complexes are considered to be beneficial for the device performance [6,10]. The presence of V_{Cu} and Zn_{Cu} in copper deficient and zinc rich $Cu_2ZnSn(SSe)_4$ has also been supported by experimental studies [13].

However, reports on solar cells with conversion efficiencies as high as 6.9% at near stoichiometric [Cu]/[Zn+Sn] ratio can also be found in the literature [14]. Although a decrease of [Cu]/[Zn+Sn] in this study improved the solar cell efficiency up to 8.1% there are studies demonstrating a deterioration of the efficiency with decreasing [Cu]/[Zn+Sn] [15,16]. These suggest that the model proposed in ref. [6] might only be valid for a limited range of CZTSe fabrication technologies whereas the defect chemistry in CZTSe is generally more complex with near stoichiometric copper content material having much potential as the absorber layer in high performance solar cells. For the successful development of efficient solar cells with near stoichiometric [Cu]/[Zn+Sn] ratios of CZTSe one should understand the chemistry of defects in such material and the influence of solar cell processing steps required for the fabrication of solar cells.

One of the most efficient experimental techniques, providing information on defects in semiconductors, is photoluminescence (PL) [17]. Low temperature PL spectra of device quality CZTSe are dominated by a broad emission band that is assigned to band-tail related recombination mechanisms [18-20]. The spectral position of such a band depends on a number of factors: the bandgap E_g, that is influenced by the degree of Cu/Zn disorder [21,22], the mean depth of the band tail as well as the type of tail-related radiative recombination [23], the energy level of the defect [13], as well as the sample temperature and excitation intensity [19,20,23,24]. It follows that accurate interpretation of PL spectra requires measurement of the bandgap. In non-transparent CZTSe films deposited on Mo/glass substrates E_g can be determined using photoluminescence excitation (PLE) spectroscopy [20,23].

Detailed PL studies of CZTSe mono-grain powder [18], thin films deposited on bare glass substrates [24] and on Mo-coated glass [20,23] as well as CZTSe-based solar cells [19] can be found in the literature. However to the best of our knowledge no reports on the influence of the solar cell processing steps, such as the KCN etching and the deposition of CdS and ZnO, on the PL or PLE spectra of CZTSe can so far be found in the literature.

In this paper we present a detailed optical spectroscopy study of CZTSe thin films (with a near stoichiometric copper content) deposited on Mo/glass substrates and explore the influence of solar cell processing steps (KCN etching, deposition of CdS and ZnO) on the PL and PLE spectra.

2. Experimental details

Molybdenum layers with a thickness of 0.85 μm were deposited on soda-lime glass substrates using magnetron sputtering. Their resistivity maps were measured using a Jandel four-point probe head along with a Keithley multimeter incorporated in a X-Y mapping system. A resistivity map of the Mo layer, measured using a Jandel four-point probe head and a Keithley multimeter in conjunction with a X-Y mapping system, is shown in Fig.1(a).

Multilayer metallic precursors, constituting a few nanometres thick alternating copper, zinc and tin layers, were sequentially deposited on the Mo-coated glass substrates (held on a rotating table) by three-target magnetron sputtering of high-purity (5N) elemental metal targets at room temperature. These precursors were then selenised in a mixture of selenium vapour with argon using a two-stage thermal annealing process. This involved heating to 300 ^{o}C for 5 minutes and then to 500 ^{o}C for 15 minutes.

The CdS buffer layer was deposited using a standard chemical bath process at 70 ^{o}C following a 0.5 min etch of the films in a 10 wt % KCN solution [14].

Solar cells were produced by depositing i-ZnO/ZnO:Al window layers at room temperature using a DC-magnetron. 3×3 mm^2 size cells were then mechanically scribed. The solar cell parameters were measured under standard test conditions (25 ^{o}C, AM1.5 and 100 mW/cm^2). The current density versus voltage parameters (J-V) were measured by directly contacting the solar cell front surface without any deposited metallic grid. The solar cells, fabricated using the films, demonstrated a conversion efficiency of 6.4% along with an open circuit voltage V_{oc} = 374 mV, short circuit current density J_{SC} = 29.7 mA cm^{-2} and fill factor FF = 56.3%. Fig.1(b) shows the J-V characteristics of the examined solar cell. More information on the deposition process and solar cell characterisation can be found elsewhere [14,20,23,24,25].

A 100 cm single grating monochromator and the unfocused 514 nm line (0.7 mm diameter) of a 300 mW Ar^+ laser were used for the PL measurements. For the PLE measurements two single grating monochromators, with focal lengths of 60 cm and 30 cm, were used to register the signal and for a tuneable source of light from a 400 W halogen lamp, respectively. The PLE spectra were measured by detecting the signal at the energy of the dominant PL band (0.8 eV). An InGaAs photomultiplier tube sensitive from 0.9 μm to 1.7 μm was used to detect the PL signal.

A closed-cycle helium cryostat was used to measure the temperature dependence of the PL spectra (from 6 K to 300 K). The PLE measurements were carried out at 4.2 K using a liquid helium bath cryostat. More experimental details can be found in ref. [20,23,24].

The morphology of the bare CZTSe films was examined by scanning electron microscopy (SEM) using a 5 keV electron beam energy. Wavelength dispersive X-ray (WDX) microanalysis was performed at a 10 keV electron beam energy.

X-ray diffraction (XRD) measurements were carried out using a D - 5000 Siemens diffractometer in the Bragg–Brentano geometry with a Cu K-$_\alpha$ radiation source (λ = 0.15406 nm).

3. Results

A dense film with grain sizes of 1 µm can be seen in the SEM cross section micrograph in Figure 1(c). A film average thickness of 1.4 µm can be estimated from the view.

WDX measurements were taken at 10 points along a line of 1 mm. The elemental composition (Cu 25.6, Zn 13.3, Sn 12.5 and Se 48.6 at.%) demonstrates a near stoichiometric ratio of copper to other metals [Cu]/[Zn+Sn] = 0.99 ± 0.02, an excess of zinc over tin [Zn]/[Sn]=1.07 ± 0.03 and a slight selenium deficiency, the ratio of Se to the sum of the metals [Se]/[Cu+Zn+Sn] = 0.94 ± 0.01. The standard deviations of the 10 measurements are taken as the error bars.

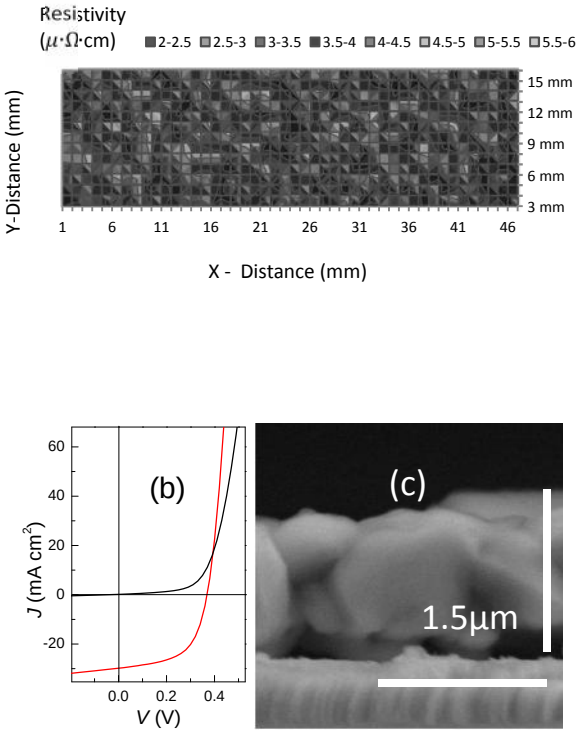

Figure 1. Resistivity map of a typical Mo layer on glass substrate (a), J-V dependencies in the dark and under illumination (b), a cross-section SEM micrograph of the CZTSe film on Mo/glass substrate (c).

The formation of a tetragonal structure of CZTSe is confirmed by the XRD pattern in Fig.2. An additional strong peak at 40^o is attributed to metallic Mo used as the back contact. This peak can be seen in the patterns from both the CZTSe/Mo and cell in Fig.2. The broad reflections at 32^o and 57^o are attributed to $MoSe_2$ due to the selenisation of molybdenum. The pattern of the cell reveals lines related to ZnO at 32^o, 34.5^o, 36^o, 47^o and 63^o. Neither of the XRD patterns reveal any significant lines of secondary phases, although ZnSe and Cu_2SnSe_3 may still be present due to similarities of their crystalline structures to that of CZTSe [3,4]. The processing changed neither the FWHM of the lines nor their intensity, suggesting that the crystalline structure has not been affected.

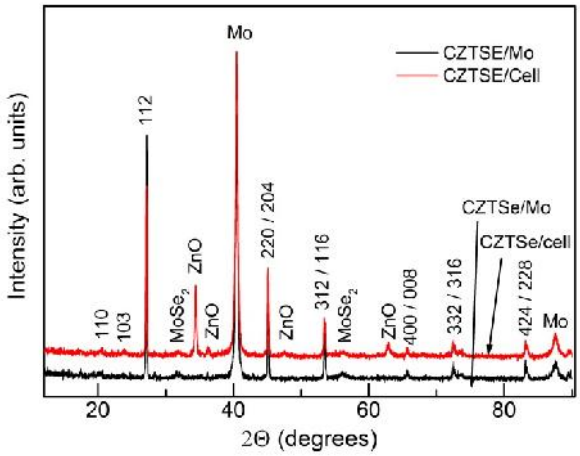

Figure 2.XRD pattern of CZTSe/ Mo and solar cell.

(a)

A comparison of the PL spectra (measured at 6 K and excitation power density of 0.32 W/cm^2) from the CZTSe/Mo/glass with that of the solar cell is shown in Fig.3(a) on a logarithmic scale.

Before device processing the PL spectra reveal a broad dominant band P1 at 0.812 eV and a low intensity band P2 at 0.936 eV. Device processing reduces the intensity of the P1 band by a factor of 2.5 whereas that of the P2 band increases by a factor of 1.5. Also, processing induces a very broad and low intensity P3 band. Its maximum intensity was observed at the verge of the detector sensitivity limit of 1.3 eV.

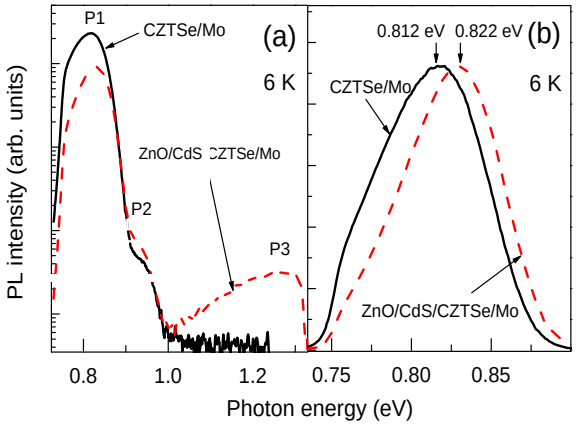

Figure 3. A comparison of the PL spectra of CZTSe/Mo before and after device processing on a logarithmic scale (a) and on a linear scale after normalisation of the P1 band (b).

The PL spectra, taken at different points across the surface, reveal similar intensities as well as shapes of

the P1, P2 and P3 bands demonstrating homogeneity of the films on a macroscale.

Fig.3(b) shows the P1 band in the PL spectra of CZTSe/Mo and solar cell on a linear scale after normalisation. It can be seen that processing blue shifts the P1 band from 0.812 eV to 0.822 eV whereas the full width at half maximum (FWHM) of the P1 band decreases after the processing from 84 meV to 76 meV. The linear scale of the PL spectra in Fig.3(b) brings out the asymmetrical shape of the P1 band. In both spectra one can see a rather steep high energy side and a gentler low energy one. The dependence of the PL spectra on the laser excitation intensity is shown in Fig.4. Increasing laser power induces significant blue shifts in the spectral position of the P1 band in both CZTSe/Mo (a) and the solar cell (b) whereas their shape does not change. The rate of this shift (*j*-shift) is 14 meV per decade of laser power change for the CZTSe/Mo film and decreases to 13 meV/decade for the cell spectra as shown in Table 1.

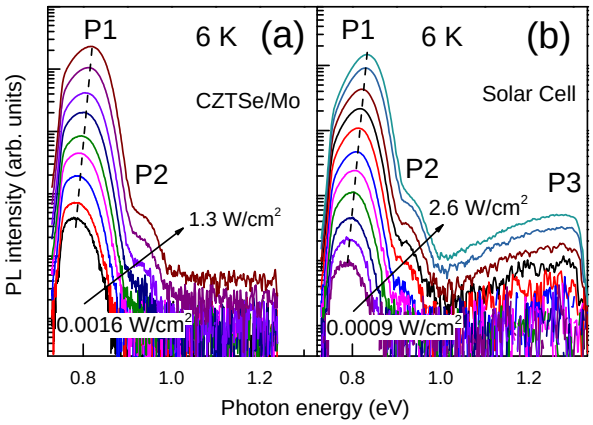

Figure 4. Excitation intensity dependencies of the PL spectra in CZTSe/Mo/glass (a) and the solar cell (b) measured at 6 K.

The characteristic asymmetric shape of the P1 band, the invariance of this shape on the excitation intensity and the significant *j*-shifts suggest that the radiative recombination mechanism of this band is associated with band tails generated by spatial potential fluctuations due to high concentrations of charged defects [18, 20, 23-27]. The P3 band in the PL spectra of the cell also increases its intensity at higher excitation. However, limitations of the detector spectral range make it difficult to determine any spectral shift of this band.

Fig.5 shows the temperature dependence of the PL spectra. The spectra from CZTSe/Mo show that the P1 band is quenched by 120 K revealing a low intensity emission band at 0.78 eV, which quenches by 140 K. The low intensity of this band, its merging with P1 and the detector range makes it difficult to analyse its nature. The P2 band can be seen to quench by 70 K.

Fig.5(b) shows the P1 band in the PL spectra of the cell up to a temperature of 200 K. It red shifts up to a temperature of 70 K and then at higher temperatures it reveals a blue shift. In the chalcopyrites [27] and kesterites [18,20,23,24] similar temperature dependencies were taken as evidence of the band-tail related nature of such transitions. As in the film the P2 band quenches by 70 K. At temperatures above 200 K the solar cell spectra show a broad band at 0.9 eV. Such bands, observed earlier in CZTS [28] and CZTSe [20,23,24], were attributed to band-to-band (BB) transitions, involving the recombination of free electrons from the conduction band with free holes from the valence band.

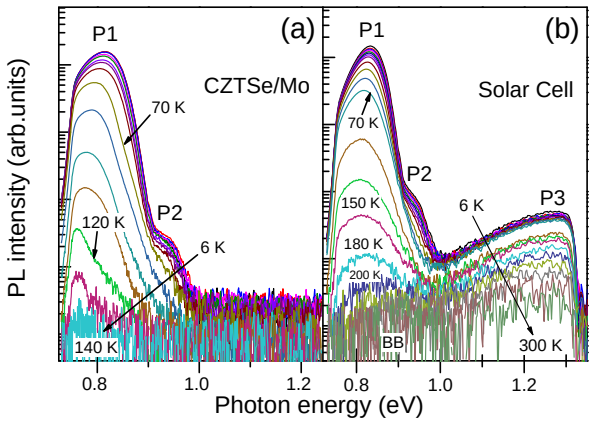

Figure 5. The temperature dependence of the PL spectra from CZTSe/Mo/glass (a) and solar cell (b).

The P3 band in the PL spectra of the solar cell gradually quenches with raising temperature however it retains a relatively high intensity up to temperatures of 300 K. High concentrations of charged defects generate tails in the density of states (DOS) of the conduction and valence bands of semiconductors. Such tails can be induced by spatial potential fluctuations [26, 27] and/ or by fluctuations of the bandgap [29].

Table 1. Spectral positions E_{max}, FWHM, *j*-shift of the P1 and P2 PL bands at 6 K and an excitation intensity of 0.8 W/cm^2, bandgaps E_g at 4.2 K, the broadening energies ΔE, average depths of potential fluctuations γ, and activation energies E_a of the temperature quenching for CZTSe/Mo and cell.

	CZTSe/Mo	**cell**
Band	**P1**	**P1**
E_{max} (eV)	0.812	0.822
FWHM (meV)	84	76
j-shift (meV/decade)	14	13
k	1.0	1.0
E_g (eV)	0.96	0.99
ΔE (meV)	33	36
γ (meV)	24	22
E_a(meV)	65±3	85±5
Band	**P2**	**P2**
E_{max} (eV)	0.936	0.928
FWHM (meV)	53	50
j-shift (meV/decade)	8	12
k	1.00	0.85
E_a(meV)	85±3	75±7

A theory of the influence of spatial potential fluctuations on the electronic properties of semiconductors [30] has been adopted to analyse PL spectra [26]. Such analysis was successfully used to interpret PL spectra of the chalcopyrites [27] and kesterites [18]. It suggests that the characteristic

asymmetric shape of the PL bands, their strong blue shift rate with increasing excitation intensity and the significant red shift with rising temperature, as observed in our PL spectra, are evidence of spatial potential fluctuations being the origin of the band tails in these spectra. Time resolved analysis of the PL emission of CZTSe [31] also suggests a potential fluctuation origin of the band tails in this material. Although we cannot totally exclude the influence of bandgap fluctuations on the formation of band-tails to interpret our results we assume the spatial potential fluctuation model [26, 27].

Thin films of CZTSe used in high performance solar cells are generally considered to have high concentrations of both donors and acceptors [3,18,20,23,31,32]. A semiconductor is highly doped if the mean distance between defects is smaller than their Bohr radii [30]. In the kesterites this condition can be satisfied more easily for electrons than for holes [33] because the theoretically estimated DOS mass of electrons $m^*_e = 0.08m_0$, whereas that of holes is greater $m^*_h = 0.21m_0$ [34]. Overlapping donor wave-functions degenerates the material in terms of donors whereas heavy holes can stay localised either at the states of the valence band tail or at acceptors which are deeper than the potential fluctuations [26,27].

PLE spectra were measured for both samples to determine the bandgap. These spectra are shown in Fig.6 along with the PL spectra. The low energy side of the PLE spectra represents the absorbance ~(E). To determine E_g this side has been fitted with sigmoidal functions proposed in [35]:

$$\sim(h\nu) = \sim_0/[1 + exp(E_g - h\nu)/aE], \qquad (1)$$

where $h\nu$ represents the photon energy, $\sim_0$ a scaling parameter and aE is a broadening parameter [36].

The best fitted curves are shown in Fig.6 by solid lines. The determined bandgap values are (0.96 ± 0.01) eV for CZTSe/Mo and (0.99 ± 0.01) eV for the solar cell, respectively, as listed in Table 1. The processing has induced a considerable increase of the bandgap by 30 meV which is also accompanied by an increase of the broadening parameter from 33 meV to 36 meV.

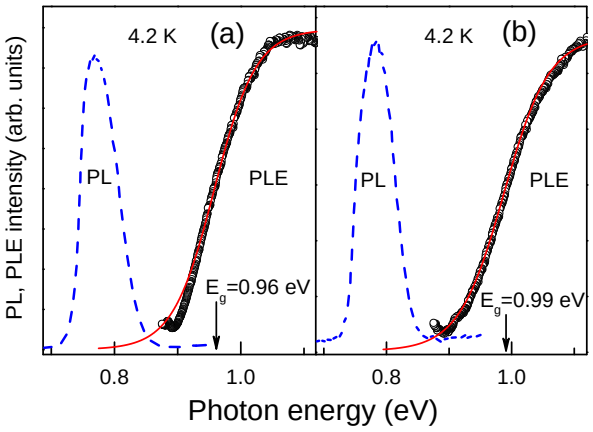

Figure 6. PLE spectra (measured at the maximum of the PL bands) of CZTSe/Mo (a), cell (b) fitted (solid lines) with sigmoidal functions.

4. Analysis of PL spectra

The possible transitions which can be found in low temperature PL spectra of highly doped semiconductors, where holes are much heavier than electrons, [26,27] are: (1) the band-to-tail (BT) recombination of holes localised at the tail of the valence band and acting like an acceptor state, with free electrons from the conduction band, (2) free-to-bound (FB) recombination of free electrons with holes localised at an acceptor with its energy level deeper than the mean depth of the band-tail.

On a microscale the spectral energy of such a level follows spatial fluctuations of the valence band so the spectral shape of such a FB band is similar to that of the BT one [36]. Such recombination bands have broad and asymmetric characteristic shapes, high j-shift and demonstrate characteristic red shift at increasing temperatures.

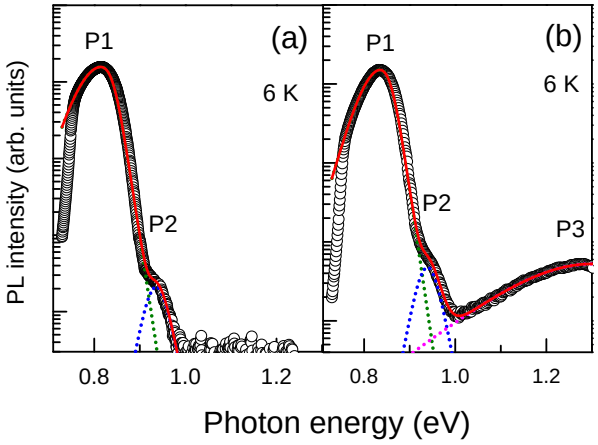

Figure 7. Experimental PL spectra (symbols) of CZTSe/Mo (a) and cell (b) taken at 6 K, fitted by DSF functions (red solid lines). The P1, P2 and P3 bands are fitted by the green, blue and magenta dotted lines, respectively.

To analyse the excitation intensity and temperature dependency of the P1, P2 and P3 bands the experimental spectra were fitted with the empirical double sigmoidal functions (DSF) proposed in [27] for BT and FB bands:

$$I(h\neg) = A\left\{1+\exp\left[-\frac{(h\neg - E_1)}{W_1}\right]\right\}^{-1} * \left\{1-\left(1+\exp\left[-\frac{(h\neg - E_2)}{W_2}\right]\right)^{-1}\right\}, \qquad (2)$$

where A, E_1, E_2, W_1 and W_2 are fitting parameters. E_1 and W_1 describe the low energy side of the band whereas E_2 and W_2 are associated with the high energy one. Examples of fitting of the PL spectra measured at 6 K are shown in Fig.7 demonstrating that the fitted DSF describe the band shape well.

DSF fitting was used to decompose the P1, P2 and P3 bands from the PL spectra in order to analyse separately their temperature and excitation intensity dependence. Such decompositions helped to estimate the spectral position of the P2 band. At 0.4 W/cm^2 laser excitation power density this was at 0.936 eV for CZTSe/Mo and 0.928 eV for the cell, with the FWHM at 53 meV and 50 meV, respectively.

The main parameters of P2 are shown in Table 1. The dependence of the spectral position of this band on the excitation power in comparison with that of P1are shown in Fig.8(a). The P1 and P2 peaks are not well resolved so the accuracy of the P2 fittings by DSF was not sufficient for further analysis.

The decomposition of P1 and P2 provides an opportunity to estimate the intensity of P2 and to compare it with that of P1. Before solar cell processing the P1 band intensity exceeded that of P2 by a factor of 600, whereas after processing, the intensity of P1 decreases and that of P2 increases, reducing the intensity ratio to about 140. A comparison of the *j*-shifts for the P1 and P2 bands is shown in Fig.8(a). In CZTSe/Mo, increasing the excitation intensity, blue shifted the P2 band at a rate of j = 8 meV per decade, which is significantly smaller than that of P1. The processing increased the *j*-shift of P2 to 12 meV/d making it closer to that of the P1 band as shown in Table 1. The dependence of the integrated intensity I of a PL band on excitation laser power P can be described as $I(P) \sim P^k$, where k is a coefficient which can be determined from the gradient of a straight line fitted to a log(I) – log(P) scale. For both the P1 and P2 bands in the CZTSe/Mo spectra the k value is found to be of 1.0. The processing does not change k for the P1 band whereas for P2 it reduced k to 0.85 as shown in Table 1. According to ref. [37] the presence of defect energy levels within the bandgap results in the involvement of these defects in radiative recombination processes reducing *k*-values below unity whereas k values greater than unity, should be taken as an indication of transitions not involving defects. A near unity value of k could be due to the presence of an unresolved BB recombination in the dominant band. The BB transition was reported in the PL spectra of CZTSe from cryogenic temperatures up to 300 K [20,23,24].

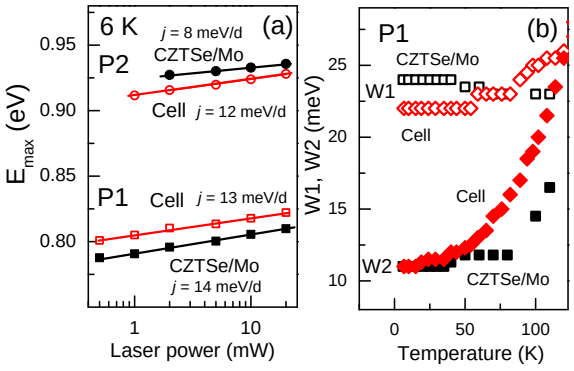

Figure 8. The dependence of spectral position E_{max} of the P1 (■-CZTSe/Mo, □-cell) and P2 (●-CZTSe/Mo, ○-cell) on the excitation intensity (a), the temperature dependence of W_1 and W_2 for the P1 bands in the PL spectra CZTSe/Mo (W_1- □, W_2-■) and cell (W_1 -◊ , W_2 - ♦)(b).

The low-energy sides of the bands are determined by the density of states (DOS) of the valence band tail °$_v$ [26,27,32] which in the case of the BT transition can be described at low temperatures by the following function:

$$\rho_v(£) \sim exp(-£ / \gamma), \qquad (3)$$

Where γ is the average energy depth of the spatial potential fluctuations in the valence band and £ is the energy from the valence band top. The FB transition is associated with the recombination of free electrons with holes localised directly at the acceptor as well as holes first localised at the valence band tail states, released and then captured at the acceptor. Potential fluctuations spread the acceptor's level to a band with a Gaussian distribution [26,32,38] so the hole density of states can be described as:

$$°_a(£) = (N_a / \sqrt{2®¥}) \exp[-(£ - I_a)^2 / 2¥^2], \qquad (4)$$

where the acceptor ionisation energy is I_a and N_a is the acceptor concentration. Thus, in both cases spatial potential fluctuations determine the low energy side of the band and its shape can be used to determine the average depth of potential fluctuations γ. To identify which of the recombination mechanisms is more likely to be present in our spectra we examine the temperature quenching of the band to find activation energies and compare them with γ. In the case when the activation energy is a fraction of γ the band can be assigned to the BT transition. If the activation energy is greater than γ then the band should be attributed to FB. The W_1 and W_2 temperature dependence of the CZTSe/Mo film and the cell are shown in Fig.8(b). Up to about 50 K, W_1 does not change much whereas W_2 gradually rises, therefore by temperatures of 100 K the P1 band becomes more symmetrical. Its shape becomes close to Gaussian due to increasing scattering of the carriers by phonons [26]. The value of W_1 at low temperatures can be taken as an estimate of γ [27] which for CZTSe/Mo is of 24 meV whereas for the cell it is of 21 meV demonstrating a slight decrease of γ due to the processing. These values are shown in Table 1.

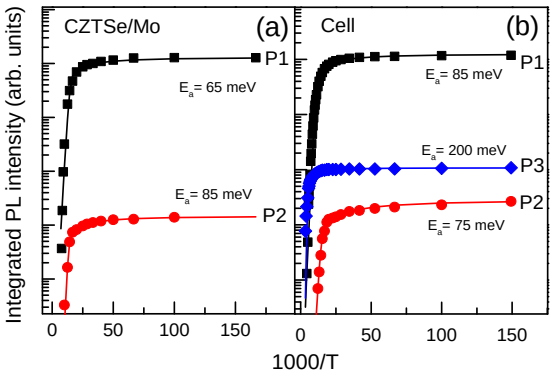

Figure 9. Arrhenius plots fitted to the integrated intensities of the bands in the PL spectra of CZTSe/Mo (a) and cell (b).

Arrhenius analysis of the temperature quenching of the P1, P2 and P3 bands was carried out assuming a single recombination channel and a dependence of the hole capture cross section on temperature [39]:

$$I(T)=I_0/\,[1+A_1T^{3/2}+A_2T^{3/2}\exp(-E_a/k_BT)], \qquad (5)$$

Where for the intensity of the analysed band I we used the integrated intensity of P1, P2 and P3. The band intensity at the lowest used temperature (6 K) is I_0, the process rate parameters are A_1 and A_2, and E_a is the process activation energy. Arrhenius fits to the experimental date points for CZTSe/Mo and the cell are shown in Fig.9. An activation energy of E_{a1} = (65±3) meV was determined for the quenching of P1 in the PL spectra of CZTSe/Mo. After processing the activation energy increases to E_{a2} = (85±3) meV. For the P2 band in the PL spectra of CZTSe/Mo E_a was determined to be (85±5) meV whereas for the cell E_a becomes (75±7) meV. The activation energies are shown in Table 1 and are all greater than γ, implying that the P1 band is likely to be associated with the FB transition, the recombination of free electrons with holes localised at an acceptor with the energy level influenced by spatial potential fluctuations. Due to the low peak intensity it was impossible to analyse the low energy side of P2 to determine γ. However, its high j-shift of 8 meV/d and red shift with rising temperature can be taken as evidence of a band-tail nature of P2. This transition was also assigned to the FB recombination of free electrons with holes captured by an acceptor with a level above the valence band that is slightly deeper than that of P1.

Only the low energy side of the P3 band can be seen in the measured PL spectra. However, the recorded part can be well fitted with the DSF shape, resulting in a maximum at 1.3 eV and FWHM of 350 meV. An example of such fitting is shown in Fig.7(b). Arrhenius analysis of the P3 temperature quenching, shown in Fig.9(b), results in E_a of (200 ± 14) meV.

5. Discussion

The reported spectral position of the dominant band in the low temperature PL spectra of CZTSe varies from 0.8 eV to 0.99 eV [15,18-21,23,24]. This position is determined by the type of PL transition and the bandgap which in turn is influenced by the degree of Cu/Zn disorder [15,21,24]. Copper vacancies can suppress the disorder [40] whereas low concentration of V_{Cu}, as expected for near stoichiometric copper content, induces a high degree of the Cu/Zn disorder. At high copper contents and an excess of zinc over tin the formation of Zn_{Cu}+Cu_{Zn} antisite defect complexes is expected. According to theoretical studies [6,41] this should result in a reduction of the bandgap. Indeed, before processing the dominant P1 band, is at about 0.81 eV in the low temperature PL spectra, whereas E_g is closer to 0.96 eV. Both values suggest a high degree of Cu/Zn disorder [22] whereas the P2 band has its spectral position blue shifted with respect to P1 by about 0.12 eV. This is consistent with a low degree of Cu/Zn disorder. The Cu/Zn disorder can be controlled by low temperature annealing reversibly changing E_a by up to 100 meV [22].

A study of CZTSe/Mo films with similar near stoichiometric [Cu]/[Zn+Sn] and excess [Zn]/[Sn] ratios demonstrated similar low temperature PL spectra with two bands: a dominant band at 0.83 eV and a low intensity one at 0.93 eV [23]. In that report the 0.83 eV band was assigned to a high degree of Zn/Cu disorder whereas the 0.93 eV band was attributed to the presence of a small fraction of CZTSe with higher degree of ordering.

The above model was used to interpret the origin of P2 in our spectra. We assumed that due to the near stoichiometric copper content and excess of zinc, the CZTSe in our films has a high degree of Cu/Zn disorder resulting in a relatively small bandgap of 0.96 eV and the P1 dominant band at 0.812 eV. However, a fraction of the CZTSe, responsible for the P2 band, has a high degree of ordering, and a larger bandgap value. The lower intensity of this band with respect to P1 (by a factor of 600) is consistent with this fraction being rather small and, therefore, PLE measurements were not reliable for the determination of its E_g. The similarity of the PL spectra at different points demonstrates the macroscale homogeneity of the films whereas on a microscopic scale the films might contain areas with a higher degree of the Cu/Zn ordering. The 8 meV/d j-shift of P2 is significantly smaller than 14 meV/decade of the P1 band. According to [26] a j-shift is associated with the compensation degree, suggesting that before device processing a small fraction of the more ordered CZTSe is less compensated. The FWHM of P2 of 53 meV is smaller than that of P1 of 84 meV which is consistent with a better structural quality of the material fraction that generated the P2 band.

Device processing changed the PL and PLE spectra. These changes include the effect of cleaning of the surface of CZTSe by removal of secondary phases with the KCN etch, the formation of the p-n junction, modification of the CdS-CZTSe interface composition by inter-diffusion of elements between the CZTSe and CdS layers and the low temperature annealing during the deposition of CdS and unintentional annealing during the deposition of ZnO.

Processing increased the bandgap by 30 meV. Such an increase is consistent with an improvement of the degree of the Cu/Zn order in the fraction of CZTSe generating P1 and can be induced by the annealing as observed in ref. [22]. Once the fraction of the CZTSe with a low degree of order becomes smaller, the intensity of P1 also becomes smaller. On the other hand, an increase of the fraction of the CZTSe with a higher degree of Cu/Zn order results in a higher intensity of P2. Although the disordered CZTSe still dominates the film, the ratio of the P1 to P2 intensities becomes smaller (140). A higher degree of Cu/Zn order after processing is consistent with a reduction of the FWHM of P1, from a value of 84 meV before device processing to 76 meV for the complete devices. The average depth of the potential fluctuation also falls from 24 meV to 22 meV after processing.

The observed increase in E_g (by 30 meV) is expected to induce a similar blue shift to the PL bands. Indeed, the P1 band has blue shifted. However, the shift of 10 meV is significantly smaller than the increase of E_g. The P1 band was assigned to the recombination of free electrons with holes localised at an acceptor. Before device processing the acceptor had a value of E_a of 65 meV, whereas after processing, E_a became 85 meV implying a change of the acceptor for one which is about 20 meV deeper. Processing also redshifted the P2 band by about 10 meV. This was accompanied by a decrease in its activation energy from 85 to 75 meV also implying a change of the main acceptor to one which is shallower and consistent with the red shift of P2. There is a possibility that such a change in the acceptor nature has a chemical origin: cadmium atoms diffuse into CZTSe changing the chemistry of defects at the CdS/CZTSe interface layer [42]. A theoretical study of the formation energy of the Cd_{Cu} antisite defects in CZTSe demonstrates that their formation energy is small although it is positive [43]. The inter-diffusion of elements at the CdS-CZTS interface takes place within a thin interface layer whereas the rest of CZTSe is not affected by Cd. This could be a reason why the observed changes in the *j*-values after the processing were relatively small. It is speculated that the greater change in the *j*-shift of the P2 band after the processing, increasing from 8 meV/d to 12 meV/d, could be due to local copper deficiency on a micro-scale resulting in a higher degree of Zn/Cu order and responsible for P2.

The deposition of *n*-type CdS on *p*-type CZTSe forms a *p*-*n* junction creating a space charge layer (SCL) in the CZTSe. Its thickness can be estimated as 0.3 µm [44]. At an absorption coefficient of $5x10^4$ cm^{-1} [45] the thickness of the layer excited by the laser can be taken as 0.2 µm suggesting that the SCL can influence the PL emission in the cells. Under the open circuit conditions of the PL measurements the photo-injected charge carriers can significantly reduce both the thickness of SCL and the magnitude of the electric field in it [46]. The action of these charge carriers is equivalent to a forward bias distorting the equilibrium electric fields. Therefore, the influence of the *p*-*n* junction on the PL spectra might be insignificant. This is supported by the similarity of the *k*-parameter of the dominant band P1 before and after the processing.

Device processing also induced a new broad band at 1.3 eV, quenching with E_a of 200 meV. This band was attributed to defects in the CdS layer.

5. Conclusion

Thin films of CZTSe, with a near stoichiometric [Cu]/[Zn+Sn] ratio, fabricated on Mo/glass substrates by the selenisation of metallic precursors, were processed to produce solar cells (V_{oc} = 374 mV, J_{sc}= 29.7 mA, *FF* = 57.7%, η = 6.4%) by KCN etching and the deposition of CdS and ZnO layers. The bandgaps of the as deposited films and solar cells was determined by PLE. PL was used to analyse the nature of the recombination. At 6 K the PL spectra of CZTSe/Mo reveal an intense band P1 at 0.81 eV and a low intensity band P2 at 0.93 eV. Their shape, high *j*-shifts with the excitation intensity change and a clear red shift at increasing temperature relate both bands to the valence band potential fluctuations with a mean depth γ of 24 meV. A comparison of their temperature quenching activation energies with γ suggests that both can be attributed to the free-to-bound recombination of free electrons with holes localised at acceptors with the energy levels spread by the potential fluctuations. It is suggested that due to its inhomogeneity CZTSe contains micro-volumes with different degrees of Cu/Zn ordering on the cation sub-lattice: a large fraction with a low degree of ordering (generating P1) and a small fraction of highly ordered Cu/Zn (generating P2). Device processing increased E_g from 0.96 eV to 0.99 eV, blue shifted P1, decreased its width, *j*-shift and γ. However device processing also decreased the P1 intensity by a factor of 2.5 whereas that of P2 increased by a factor of 1.5. These changes suggest an improvement of the structural quality of CZTSe, which can partly be attributed to the effect of cleaning the film by KCN etching, the chemical effect of Cd diffusing and filling copper vacancies at the CdS-CZTSe interface layer, and/or low temperature annealing due to the CdS and ZnO deposition increasing the fraction of CZTSe with a high degree of Cu/Zn ordering (raising the intensity of P2).

Acknowledgement

This research was supported by the Russian Science Foundation (grant No 17-12-01500). The interpretation of the experiments was partly supported by institutional research funding IUT (IUT19-28) of the Estonian Ministry of Education and EU Regional Development Fund (project TK141).

References

[1] Liu X, Feng Y, Cui H, Liu F, Hao X, Conibeer G, Mitzi D B, Green M 2016 The current status and future prospects of kesterite solar cells: a brief review *Prog. Photovolt., Res. Appl.* **24** 879–98

[2] Lee Y S, Gershon T, Gunawan O, Todorov T K, Gokmen T, Virgus Y, Guha S 2015 $Cu_2ZnSnSe_4$ Thin-Film Solar Cells by Thermal Co-evaporation with 11.6% Efficiency and Improved Minority Carrier Diffusion Length *Adv. Energy Mater.* **12** 1401372

[3] Siebentritt S, Schorr S 2012 Kesterites - a challenging material for solar cells *Prog. Photovolt., Res. Appl.* **20** 512-19

[4] Schorr S, Hoebler H J, Tovar M 2007 A neutron diffraction study of the stannite–kesterite solid solution series *European J. Mineralogy* **19** 65–73

[5] Romero M J, Du H, Teeter G, Yan Y, Al-Jassim M M 2011 Comparative study of the luminescence and intrinsic point defects in the kesterite Cu_2ZnSnS_4 and chalcopyrite $Cu(In,Ga)Se_2$ thin films used in photovoltaic applications *Phys. Rev. B* **84** 165324

[6] Chen S, Walsh A, Gong X G, Wei S H 2013 Classification of lattice defects in the kesterite Cu_2ZnSnS_4 and $Cu_2ZnSnSe_4$ earth-abundant solar cell absorbers *Adv.Mater.* **25** 1522-39

[7] Kim J and Shin B 2017 Strategies to Reduce the Open-Circuit Voltage Deficit in Cu2ZnSn(S,Se)4 Thin Film Solar Cells *Electron. Mater. Lett.* **13** 373-92

[8] Winkler M T, Wang W, Gunawan O, Hovel H J, Todorov T K, Mitzi D B 2009 Optical designs that improve the efficiency of $Cu_2ZnSn(S,Se)_4$ solar cells *Thin Solid Films* **517** 2455-60

[9] Zhang S B, Wei S-H, Zunger A 1998 Defect physics of the $CuInSe_2$ chalcopyrite semiconductor *Phys. Rev. B* **57** 9642-56

[10] Dimitrievska M, Fairbrother A, Saucedo E, Perez-Rodriguez A, Izquierdo-Roca V 2015 Influence of compositionally induced defects on the vibrational properties of device grade $Cu_2ZnSnSe_4$ absorbers for kesterite based solar cells *Appl. Phys. Lett.* **106** 073903

[11] Haass S G, Diethelm M, Werner M, Bissig B, Romanyuk Y E, Tiwari A N 2015 11.2% Efficient Solution Processed Kesterite Solar Cell with a Low Voltage Deficit *Adv. Energy Mater.* **5** 1500712

[12] Lafond A, Choubrac L, Guillot-Deudon C, Deniard P, Jobic S 2012 Crystal Structures of Photovoltaic Chalcogenides, an Intricate Puzzle to Solve: the Cases of CIGSe and CZTS Materials *Z. Anorg. Allg. Chem.* **638** 2571

[13] Tiwari D, Skidchenko E, Bowers J W, Yakushev M V, Martin R W, Fermin D J 2017 Spectroscopic and Electrical Signatures of Acceptor States in Solution Processed $Cu_2ZnSn(S,Se)_4$ Solar Cells *J. Mater. Chem. C* **5** 12720-7

[14] Márquez J, Neuschitzer M, Dimitrievska M, Gunder R, Haass S, Werner M, Romanyuk Y E, Schorr S, Pearsall N M, Forbes I 2016 Systematic compositional changes and their influence on lattice and optoelectronic properties of $Cu_2ZnSnSe_4$ kesterite solar cells *Sol. Energy Mater. Sol. Cells* **144** 579-85.

[15] Lang M, Renz T, Mathes N, Neuwirth M, Schnabel T, Kalt H, Hetterinh M 2016 Influence of the Cu Content in $Cu_2ZnSn(S,Se)_4$ solar cell absorbers on order-disorder related band gap changes *Appl. Phys. Lett.* **109** 142103

[16] Demircioğlu O, Salas J F L, Rey G, Weiss T, Mousel M, Redinger A, Siebentritt S, Parisi J, Gütay L 2017 Optical properties of $Cu_2ZnSnSe_4$ thin films and identification of secondary phases by spectroscopic ellipsometry *Optics Express* **25** 5327-5340

[17] Bebb H B and Williams E 1972 Semiconductors and Semimetals (New York: Academic Press)

[18] Grossberg M, Krustok J, Timmo K, Altosaar M 2009 Radiative recombination in $Cu_2ZnSnSe_4$ monograins studied by photoluminescence spectroscopy *Thin Solid Films* **517** 2489-92

[19] Oueslati S, Brammertz G, Buffiere M, Koble C, Oualid T, Meuris M, Poortmans J 2015 Photoluminescence study and observation of unusual optical transitions in $Cu_2ZnSnSe_4$/CdS/ZnO solar cells *Sol. Energy Mater. Sol. Cells* **134** 340-45

[20] Márquez-Prieto J, Yakushev M V, Forbes I, Krustok J, Zhivulko V D, Edwards P R, Dimitrievska M, Izquerdo-Roca V, Pearsall N M, Mudryi A V, Martin R W 2016 Impact of the selenisation temperature on the structure and optical properties of CZTSe absorbers *Sol. Energy Mater. Sol. Cells* **152** 42-50

[21] Rey A R G, Sendler J, Weiss T P, Thevenin M, Guennou M, El Adib B, Siebentritt S 2014 The band gap of Cu2ZnSnSe4: Effect of order-disorder *Appl. Phys. Lett.***105** 112106

[22] Krämmer C, Huber C, Zimmermann C, Lang M, Schnabel T, Abzieher T, Ahlswede E, Kalt H, Hetterich M 2014 Reversible order-disorder related band gap changes in $Cu_2ZnSn(S,Se)_4$ via post-annealing of solar cells measured by electroreflectance *Appl. Phys. Lett.* **105** 262104

[23] Yakushev M V, Sulimov M A, Márquez-Prieto J, Forbes I, Krustok J, Edwards P R, Zhivulko V D,. Borodavchenko O M, Mudryi A V, Martin R W 2017 Influence of the copper content on the optical properties of CZTSe thin films *Sol. Energy Mater. Sol. Cell* **168** 69-77

[24] Yakushev M V, Márquez-Prieto J, Forbes I, Edwards P R, Zhivulko V D, Mudryi A V, Krustok J, Martin RW 2015 Radiative recombination in $Cu_2ZnSnSe_4$ thin films with Cu deficiency and Zn excess *J. Phys. D: Appl. Phys.* **48** 475109

[25] Zoppi G, Forbes I, Miles R W, Dale P J, Scragg J J and Peter L M 2009 $Cu_2ZnSnSe_4$ Thin Film Solar Cells Produced by Selenisation of Magnetron Sputtered Precursors, *Prog. Photovolt, Res. Appl.* **17** 315–19

[26] Levanyuk A P, Osipov V V 1981 Edge Luminescence of the Direct Gap Semiconductors *Usp. Fiz. Nauk.* **133** 427-77.

[27] Krustok J, Collan H, Yakushev M, Hjelt K 1999 The role of spatial potential fluctuations in the shape of the PL bands of multinary semiconductor compounds *Physica Scripta* **T79** 179-182

[28] Grossberg M, Salu P, Raudoja J, Krustok J 2013 Micro-photoluminescence study of Cu_2ZnSnS_4 polycrystals *J. Photon. Energy* **3** 030599

[29] Mattheis J, Rau U, Werner I H 2007 Light absorption and emission in semiconductors with band gap fluctuations - A study on $Cu(In,Ga)Se_2$ thin films *J. Appl. Phys.* **101** 113519

[30] Shklovskii B, Efros 1984 A Electronic Properties of Doped Semiconductors (Berlin: Springer)

[31] Gokmen T, Ganawan O, Todorov T K, Mitzi D B 2013 Band Tailing and Efficiency Limitations in Kesterita Solar Cells *Appl. Phys. Lett.* **103** 103506

[32] Siebentritt S, Papathanasioua N, Lux-Steiner M Ch 2006 Potential fluctuations in compensated chalcopyrites, *Physica B* **376-377** 831-3

[33] Teixeira J P, Sousa R A, Sousa M G, Cunha A F, P. A. Fernandes, Salome P M P, Leitao J P 2014 Radiative transitions in highly doped and compensated chalcopyrites and kesterites: The case of Cu_2ZnSnS_4 *Phys. Rev. B* **90** 235202

[34] Persson C 2010 Electronic and optical properties of Cu_2ZnSnS_4 and $Cu_2ZnSnSe_4$ *J. Appl. Phys.* **107** 053710

[35] O'Donnell K P, Martin R W, Middleton P G 1999 Origin of luminescence from InGaN Diodes *Phys. Rev. Lett*. **82** 237-40.

[36] White M E, O'Donnell K P, Martin R W, Pereira S, Deatcher C J, Watson I M 2002 Photoluminescence excitation spectroscopy of InGaN epilayers *Mater. Science and Engin*. B **93** 147–49.

[37] Schmidt T, Lischka K, Zulehner W 1992 Excitation-power dependence of the near-band-edge photoluminescence of semiconductors *Phys. Rev. B* **45** 8989-94.

[38] Jagomagi A, Krustok J, Raudoja J, Grossberg M, Danilson M, Yakushev M 2003 Photoluminescence studies of heavily doped $CuInTe_2$ crystals *Physica B* **337** 369-374

[39] Krustok J, Collan H, Hjelt K 1997 Does the low-temperature Arrhenius plot of the photoluminescence intensity in CdTe point towards an erroneous activation energy? *J. Appl. Phys*. **81** 1442-5.

[40] Paris M, Choubrac L, Lafond A, Guillot-Deudon C, Jobic S 2014 Solid-state NMR and Raman spectroscopy to address the local structure of defects and the tricky issue of the Cu/Zn disorder in Cu-poor, Zn-rich CZTS materials *Inorganic Chemistry* **53** 8646-53

[41] Huang D, Persson C. 2013 Band gap change induced by defect complexes in Cu_2ZnSnS_4, *Thin Solid Films* **535** 265-69

[42] Bar M, Repins I, Weinhardt L, Alsmeier J-H, Pookpanratana S, Blum M, Yang W, Heske C, Wilks R G, Noufi R 2017 Zn−Se−Cd−S Interlayer Formation at the $CdS/Cu_2ZnSnSe_4$ Thin-Film Solar Cell Interface *ACS Energy Lett*. **2** 1632

[43] Maeda T, Nakamura S, Wada T 2012 First-Principles Study on Cd Doping in Cu_2ZnSnS_4 and $Cu_2ZnSnSe_4$ *Jap. J. Appl. Phys.* **51** 10NC11-6.

[44] Ranjbar S, Brammertz G, Vermang B, Hadipour A, Sylvester M, Mule A, Meuris M, Cunha A F, Poortmans J 2017 Effect of Sn/Zn/Cu precursor stack thickness on two-step processed kesterite solar cells *Thin Solid Films* **633** 127-30

[45] Amal M I, Kim K H 2012 Optical properties of selenised $Cu_2ZnSnSe_4$ films from a Cu-Zn-Sn metallic precursor *Chalcogenide Lett*. **9** 345–53

[46] Metzger W K, Ahrenkiel R K, Dashdorj J,. Friedman D J 2005 Analysis of charge separation dynamics in a semiconductor junction *Phys. Rev. B* **71** 035301